# Optimization of Protection and Regulation Strategies to Maintain System Stability in the Presence of Symmetrical Voltage Dips in DFIG Wind Turbines

**Medjadji Nassira[1], Medjahed Driss Meddah[2] , Mahammedi Abdelkader[3] ,**

**Kaddour Abdelmadjid[4*] , Tlili Salah[5] , Nettari Mohammed[5]**

[1] Electrical Engineering Department, University Center Salhi Ahmed Naama (Ctr. Univ. Naama), P.O. Box 66, Naama 45000, Algeria

[2].Mechanical Engineering Department, University Center Salhi Ahmed Naama (Ctr. Univ. Naama), P.O. Box 66, Naama 45000, Algeria

[3] Department of Technology, Ziane Achour University of Djelfa, 17000 Djelfa, Algeria

[4] *Unité de Recherche Appliquée en Energies Renouvelables, URAER, Centre de Développement des Energies Renouvelables, CDER, 47133, Ghardaïa, Algeria

[5] Univ. Ouargla, Fac. Mathematics and Material Sciences, Lab.. Development Of New And Renewable Energies In Arid And Saharan Zones Laboratory (LARENZA), Algeria

[*] ***Email corresponding author:*** *kaddour.majid@gmail.com*

**Received: June 06, 2023 Revised: August 20, 2023 Accepted: September 03, 2023 Published: September 16, 2023**

**Abstract**

Symmetrical voltage dips, are frequent in power systems, impacting wind turbines, especially DFIG-equipped ones. This study focuses on optimizing protection and regulation to ensure stability during these dips. It examines DFIG behavior during voltage dips, proposes effective control strategies, and validates them through simulations. Results confirm successful dip mitigation without major turbine stability or power output disruptions. These findings enhance DFIG-based wind turbines' reliability and performance, offering insights for manufacturers and operators to improve wind energy systems

**Keywords:** - Symmetrical Voltage Dips, wind turbines, DFIG, system stability, crowbar protection.

**Tob Regul Sci. ™ 2023;9(1): 5240 - 5262**
**DOI: doi.org/10.18001/TRS.9.1.364**

## Introduction

Wind farms play an increasingly important role in renewable energy production [1-2]. Among the various types of wind turbines, those equipped with a doubly fed induction generator (DFIG) are widely used due to their advantages in terms of energy efficiency and power control [3-4]. However, these systems are susceptible to disturbances such as symmetrical voltage dips, which can affect their stability and performance [5].

Symmetrical voltage dips occur when the voltage of the electrical grid drops abruptly for a short period. These disturbances can be caused by events such as short circuits, grid failures, or the operation of other electrical equipment [6-7]. Symmetrical voltage dips can lead to transient variations in the electrical and mechanical quantities of the DFIG, which can impact its stability and ability to provide constant power to the grid [8-9].

In this work, we focus on optimizing crowbar protection strategies and regulation to maintain the stability of the DFIG system in the presence of symmetrical voltage dips. We examine crowbar protection approaches, such as the use of crowbar resistors, which help maintain the connection of the wind turbine to the grid during periods of symmetrical voltage dips. We also analyze the regulation strategy that minimizes transient effects on the rotor speed and ensures stable system operation.

The objective of this study is to optimize control parameters, such as the settings of the rotor-side and grid-side converters, to ensure a rapid and efficient response to symmetrical voltage dip. We aim to maximize wind energy production while ensuring system stability and equipment protection.

This study contributes to the understanding the challenges associated with integrating DFIG wind turbines into electrical grids, as well as identifying optimal solutions to ensure their stability and operational efficiency. The findings of this research can be utilized by wind farm designers and grid operators to enhance the reliability and performance of DFIG wind systems under disturbance conditions such as symmetrical voltage dips."

To achieve these goals, we utilize advanced simulation tools such as MATLAB and Simulink to model the DFIG system and evaluate the effectiveness of the crowbar protection and regulation strategies. We analyze the obtained results and provide recommendations to improve system performance in the presence of symmetrical voltage dips.

## 1.Description of a wind energy conversion system based on a DFIG

We begin with the description of the different components comprising a wind turbine based on the Doubly Fed Induction Generator (DFIG), which is widely used as a wind energy source due to its flexibility and high performance, as depicted in Figure 1. The mechanical part of the system consists of the turbine, gearbox, and shaft. In Figure 1, the second part represents the generator, and in part three, we have the back-to-back converter along with its controls. The control of the system consists of:

01-Power Maximization Block: Maximum Power Point Tracking (MPPT)

02-RSC control block: Rotor-side converter

03-GSC control block: Grid-side converter

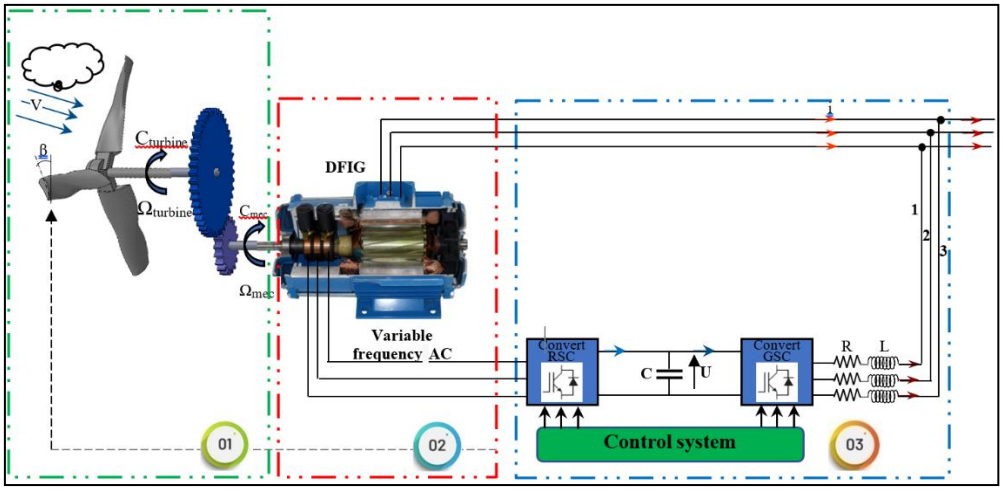


**Fig 1. General Structure of the Different Parts of the System**

## 2.Modeling of the wind turbine

A wind turbine is a device that converts the kinetic energy of the wind into mechanical or electrical energy. It typically consists of a rotor with blades, a generator, and supporting structures such as a tower (figure 2).

### a-Mechanical power of the turbine

The kinetic power of the wind is given by the following equation:

$$P_{incident} = \frac{1}{2}.\rho.S.V^3 \qquad (1)$$

Where:

$\rho$: air density [kg/m^3]

$S$: swept area of the rotor [m^2], $V$: wind speed [m/s].

The aerodynamic power extracted from the wind can be described as follows.

$$P_{incident} = \frac{1}{2}.\rho.\pi.R^2.C_p(\lambda,\beta).V_{wind}^3 \quad (2)$$

$V_{wind}$: wind power [W]

$P_{incident}$:aerodynamique wind turbine power [W]

$R$: Turbine radius [m]

$\rho$ :Air density [kg/m^3]

$C_p$: Coefficient of power

$\lambda$: Relative speed [m/s]

$\beta$: Blade pitch angle in degrees (°)

**b-Power coefficient Cp**

The power coefficient Cp represents the aerodynamic efficiency of the wind turbine and is influenced by its characteristics. This coefficient is determined by the ratio of the speed and angle of orientation of the blade.

$$\begin{cases} C_p = (c_1 - c_2)(\beta - c_3)\sin(A) - c_4(\lambda - c_5)(\beta - c_3) \\ A = \frac{\pi(\lambda+0.1)}{18.5-0.3(\beta-2)} \end{cases} \quad (3)$$

Where the values of the chosen coefficients of c1-c5 are:

**Table 1. Coefficient values**

| $c_1$ | $c_2$ | $c_3$ | $c_4$ | $c_5$ |
|---|---|---|---|---|
| 0.5 | 0.167 | 2 | 0.00184 | 3 |

**c-Relative speed λ**

To facilitate the practical utilization of the power coefficient Cp, we introduce a variable known as the relative speed, which is defined by the following expression.

$$\lambda = \frac{\Omega_{turb}.R}{V_{vent}} \quad (4)$$

**d-Mechanical torque of the turbine**

Based on the equation for the power generated by the turbine and the knowledge of the turbine's rotational speed, the mechanical torque can be expressed as follows.

$$C_{aer} = \frac{P_{aer}}{\Omega_{turb}} = \frac{1}{2}.\rho.\pi.R^2.C_p(\lambda,\beta).V_{wind}^3.\frac{1}{\Omega_{turb}} \qquad (5)$$

**e-Gearbox model**

The gearbox is responsible for converting the mechanical speed of the turbine into the speed required by the generator, as well as transmitting the aerodynamic torque as the driving torque of the generator. This transformation is achieved through a series of mathematical formulas as outlined below.

$$G = \frac{\Omega}{\Omega_{turb}} \; ; \; G = \frac{C_{turb}}{C_m} \qquad (6)$$

With:

$G$: Gear ratio, $C_{aer}$: Aerodynamic torque of the turbine (N.m),

$\Omega_{turb}$: Turbine speed (rad/s), $\Omega$: Generator speed (rad/s), $C_m$: Generator torque (N.m).

**f-Driveshaft dynamic equation**

The fundamental equation of dynamics allows us to determine the evolution of the mechanical speed based on the mechanical torque applied to the rotor shaft of the wind turbine ($C_m$) and the electromagnetic torque ($C_{em}$).

$$J\frac{d\Omega}{dt} = C_m - C_{em} - B.\Omega \qquad (7)$$

**h-The total inertia J**

consists of the inertia of the turbine referred to the high-speed axis and the inertia of the generator [16].

$$J = \frac{J_{turb}}{G} + J_m \qquad (8)$$

with

– $C_{em}$: electromagnetic torque [Nm],

– $J_{turb}$: inertia of the turbine [kg:m2],

– $J_m$: generator inertia [kg:m2].

From the previous equations the block diagram corresponding to this modeling of the turbine is given by figure 2.

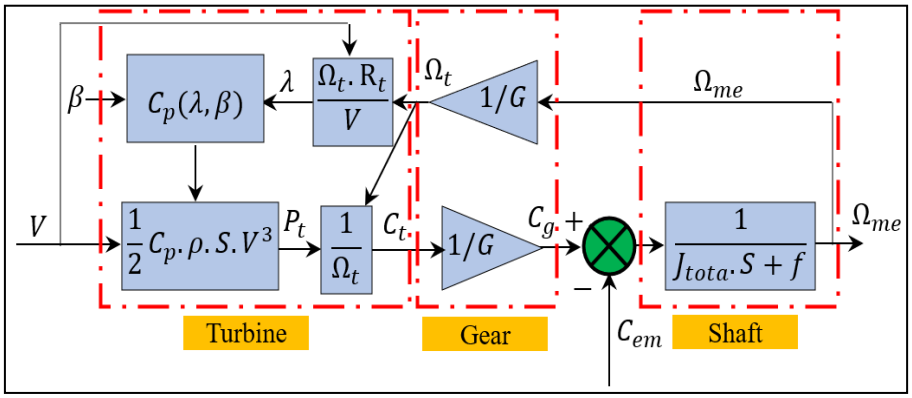


Fig 2. Block diagram of the wind converter mode

## 3-Modeling of the Doubly Fed Induction Generator (DFIG)

The mathematical model of the Doubly Fed Induction Generator (DFIG) is expressed in the reference frame (d-q) rotating at the speed of the stator field. This model is based on the following equations [10-15].

### a-Electrical equations of stator voltages

$$\begin{cases} V_{sd} = R_s i_{sd} + \frac{d\varphi_{sd}}{dt} - \frac{d\theta_s}{dt}\varphi_{sq} \\ V_{sq} = R_s i_{sq} + \frac{d\varphi_{sq}}{dt} + \frac{d\theta_s}{dt}\varphi_{sd} \end{cases} \quad (9)$$

### b-Electrical Equations of Rotor Voltages

$$\begin{cases} V_{rd} = R_r i_{rd} + \frac{d\varphi_{rd}}{dt} - \frac{d\theta_r}{dt}\varphi_{rq} \\ V_{rq} = R_r i_{rq} + \frac{d\varphi_{rq}}{dt} + \frac{d\theta_r}{dt}\varphi_{rd} \end{cases} \quad (10)$$

### c-Magnetic Equations of Stator Fluxes

$$\begin{cases} \varphi_{sd} = L_s i_{sd} + M_{sr} i_{rd} \\ \varphi_{sq} = L_s i_{sq} + M_{sr} i_{rq} \end{cases} \quad (11)$$

### d-Magnetic Equations of Rotor Fluxes

$$\begin{cases} \varphi_{rd} = L_r i_{rd} + M_{sr} i_{sd} \\ \varphi_{rq} = L_r i_{rq} + M_{sr} i_{sq} \end{cases} \quad (12)$$

### e-Electromagnetic torque equation

Using the modified Park transformation, which preserves the instantaneous power invariance, the expression of the electromagnetic torque in the (d-q) reference frame can be given as follows:

$$V_{rq} = \left[V_{s_{A,B,C}}\right]^T \cdot \left[I_{s_{A,B,C}}\right] + \left[V_{r_{A,B,C}}\right]^T \cdot \left[I_{r_{A,B,C}}\right] = \left[V_{s_{d,q}}\right]^T \cdot \left[I_{s_{d,q}}\right] + \left[V_{r_{d,q}}\right]^T \cdot \left[I_{r_{d,q}}\right] \quad (13)$$

$$P_e = \left[V_{s_{A,B,C}}\right]^T \cdot \left[I_{s_{A,B,C}}\right] + \left[V_{r_{A,B,C}}\right]^T \cdot \left[I_{r_{A,B,C}}\right] = \left[V_{s_{d,q}}\right]^T \cdot \left[I_{s_{d,q}}\right] + \left[V_{r_{d,q}}\right]^T \cdot \left[I_{r_{d,q}}\right] \quad (14)$$

By expanding the right-hand side and substituting the direct and quadrature components of the voltages, the following expression is obtained.

$$P_e = R_s.\left[i_{sd}^2 + i_{sq}^2\right] + R_r.\left[i_{rd}^2 + i_{rq}^2\right] + \left[\frac{d\varphi_{sd}}{dt}.i_{sd} + \frac{d\varphi_{sq}}{dt}.i_{sq}\right] + \left[\frac{d\varphi_{rd}}{dt}.i_{rd} + \frac{d\varphi_{rq}}{dt}.i_{rq}\right] + \left[\left(\varphi_{sd}.i_{sd} - \varphi_{sq}.i_{sd}\right).\frac{d\theta_s}{dt}\right] + \left[\left(\varphi_{rd}.i_{rq} - \varphi_{rq}.i_{rd}\right).\frac{d\theta_r}{dt}\right] \quad (15)$$

The electromagnetic torque is determined based on the following relationship:

$$P_{em} = \frac{P_{em}}{\Omega_s} \quad (16)$$

Knowing that:

$$\frac{d\theta_s}{dt} = \omega_s = p.\Omega_s \quad (17)$$

Other expressions can be established based on the chosen variables:

$$C_{em} = p.\frac{M_{sr}}{L_s}.\left(\varphi_{sq}.i_{rd} - \varphi_{sd}.i_{sd}\right) \quad (18)$$

Finally, to complete the model, the fundamental equation of dynamics is added to account for the influence of the various torques exerted on the rotor shaft:

$$C_{em} = J.\frac{d\Omega}{dt} + C_r \quad (19)$$

Where J and Cr represent the moment of inertia and the resisting torque applied to the machine shaft.

The active and reactive powers of the stator are defined by the following relationships.

$$\begin{cases} P_s = v_{sd}.i_{sd} + v_{sq}.i_{sq} \\ Q_s = v_{sq}.i_{sd} - v_{sd}.i_{sq} \end{cases} \quad (20)$$

Similarly, the powers of the rotor are given by the following expressions:

$$\begin{cases} P_r = v_{rd}.i_{rd} + v_{rq}.i_{rq} \\ Q_r = v_{rq}.i_{rd} - v_{rd}.i_{rq} \end{cases} \quad (21)$$

Taking into account the magnetic equations (20) and (21), the system of electrical equations becomes:

$$\begin{cases} v_{sd} = \left(R_s + L_s.\frac{d}{dt}\right).i_{sd} + M_{sr}\frac{di_{rd}}{dt} - L_s\omega_s i_{sq} - M_{sr}\omega_s i_{rq} \\ v_{sq} = \left(R_s + L_s.\frac{d}{dt}\right).i_{sq} + M_{sr}\frac{di_{rq}}{dt} - L_s\omega_s i_{sd} - M_{sr}\omega_s i_{rd} \\ v_{rd} = \left(R_r + L_r.\frac{d}{dt}\right).i_{rd} + M_{sr}\frac{di_{sd}}{dt} - L_r\omega_r i_{rq} + M_{sr}\omega_r i_{sq} \\ v_{rq} = \left(R_r + L_r.\frac{d}{dt}\right).i_{rq} + M_{sr}\frac{di_{sq}}{dt} - L_r\omega_r i_{rd} + M_{sr}\omega_r i_{sd} \end{cases} \quad (22)$$

This reference system is Figure 3 illustrates the schematic representation of the machine equations. This reference system is well-suited for the synthesis of the control strategy proposed in this study.

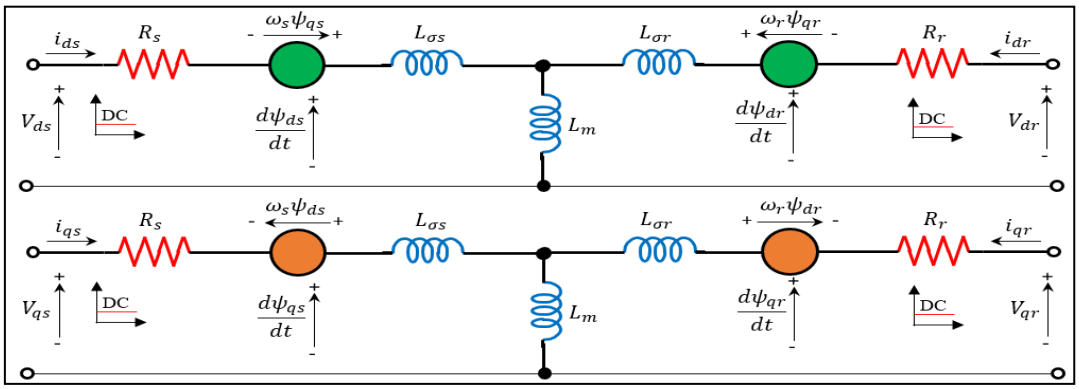


Fig 3. Model of DFIM in dq reference frame

## Control System of Rotor Side Converter and Grid Side Converter

The Power Maximization Block is responsible for implementing Maximum Power Point Tracking (MPPT) algorithms. MPPT ensures that the wind turbine operates at its maximum power output by continuously adjusting the generator's operating point to match the varying wind conditions.

## Rotor Current Control Loops

However, Figure 4 demonstrates that when equal proportional-integral (PI) regulators are chosen for both current control loops [16].

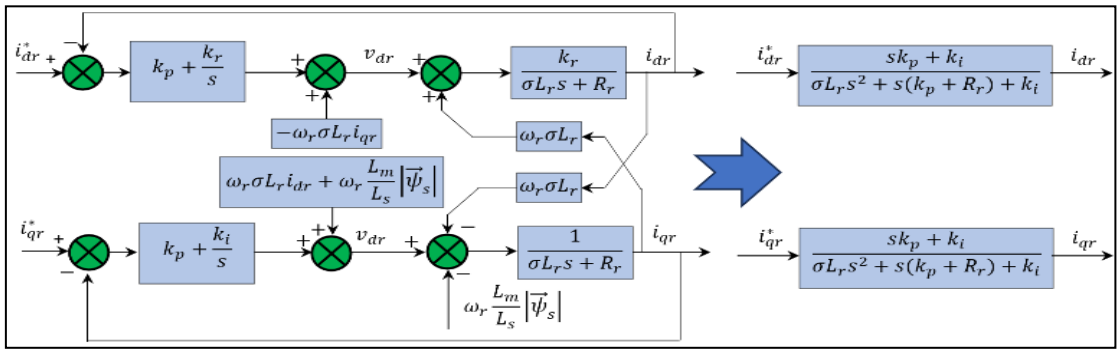


Fig 4. system of closed loop current control with PI regulator

## Power and Speed Control Loops

The torque expression in the dq frame can be simplified as follows:

$$T_{em} = \frac{3}{2} P \frac{L_m}{L_s} \left(\psi_{qs} i_{dr} - \psi_{ds} i_{qr}\right) \Rightarrow T_{em} = -\frac{3}{2} P \frac{L_m}{L_s} \left|\vec{\psi}_s\right| i_{qr} \Rightarrow T_{em} = K_T i_{qr} \quad (23)$$

When the iqr current is combined with the torque, it allows for the control of both the torque and the machine's speed.

Similarly, by expanding the expression of the stator reactive power in the dq reference frame, we obtain the expression of Qs based on idr:

$$Q_s = \frac{3}{2}\left(v_{qs} i_{ds} - v_{ds} i_{qs}\right) \Rightarrow Q_s = -\frac{3}{2} \omega_s \frac{L_m}{L_s} \left|\vec{\psi}_s\right| \left(i_{dr} - \frac{\left|\vec{\psi}_s\right|}{L_m}\right) \Rightarrow Q_s = K_Q \left(i_{dr} - \frac{\left|\vec{\psi}_s\right|}{L_m}\right) \quad (24)$$

Figure 5 illustrates the complete vector control of the DFIM. By maintaining the current loops, a speed loop, and a stator reactive power loop, it is possible to control the magnetization of the machine.

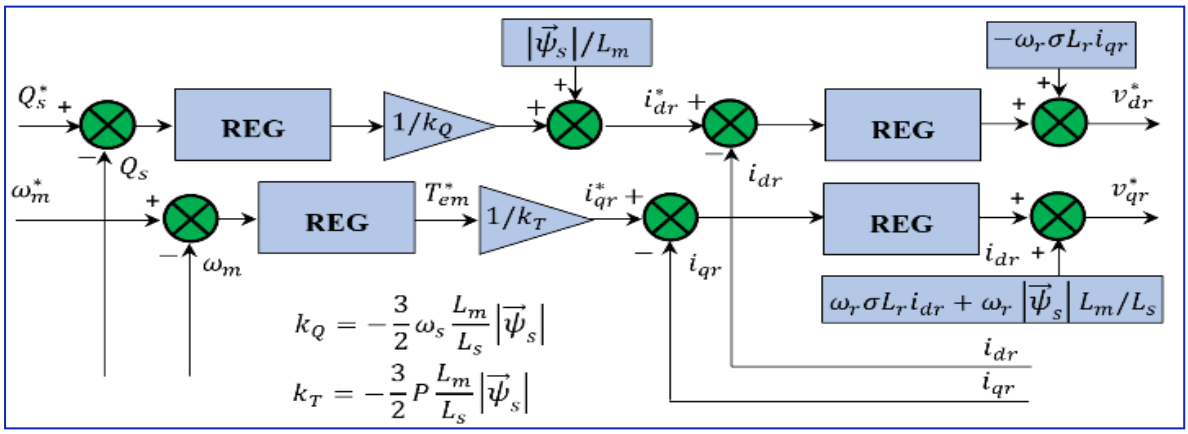


**Fig 5. complete vector control of dfig**

The dq model of the DFIM is useful for developing the stator flux-oriented vector control strategy. The DFIM is required to operate according to the given demands of Tem, ωm, and Qs. The task is to deduce the remaining interesting electrical quantities of the machine in steady-state, such as stator and rotor currents, powers, and slip.

Such as: The stator is directly connected to the grid, while the rotor is supplied by a bidirectional converter that is also connected to the grid (Figure 5).

The back-to-back converter, utilizing vector control techniques, enables energy generation at the nominal grid frequency and voltage, regardless of the rotor speed [17].

### 1-The RSC control block

Refers to the control system for the Rotor-Side Converter (RSC). The RSC is responsible for controlling the power flow between the rotor of the generator and the DC link. It regulates the rotor currents and allows for the efficient extraction of power from the wind.

### 2-The GSC control block

Represents the control system for the Grid-Side Converter (GSC). The GSC is responsible for controlling the power flow between the DC link and the grid. It ensures the synchronization of the generator's output with the grid's voltage and frequency, and it regulates the active and reactive power injected into the grid.

### 3-Crowbar Protection

Voltage dips, also known as sudden drops in grid voltage, are caused by contingencies or faults in the electricity grid. This study focuses specifically on symmetric voltage dips. In compliance with grid codes, wind turbines are required to have low voltage ride-through (LVRT) capability, meaning they must remain connected to the grid during significant voltage dips. To protect the system from overcurrents and overvoltages that may occur during the dip, a crowbar is utilized. The crowbar is connected to the rotor and is activated and deactivated without disconnecting the Doubly Fed Induction Generator (DFIG) from the grid.

When the crowbar is connected to the rotor to protect the Rotor Side Converter (RSC), as shown in Figure 6.

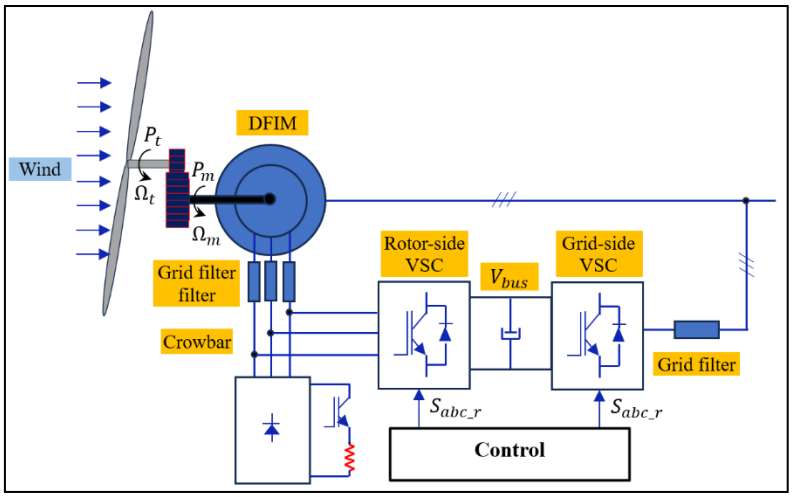


**Fig 6.** System equipped with crowbar protection.

The complete simulation of the wind system, based on a DFIG powered by a back-to-back converter with crowbar protection, is depicted in the following figure (figure 7). In order to achieve a reliable solution for symmetrical voltage dips, the SimPowerSystem toolbox was utilized to conduct all the simulations [16].

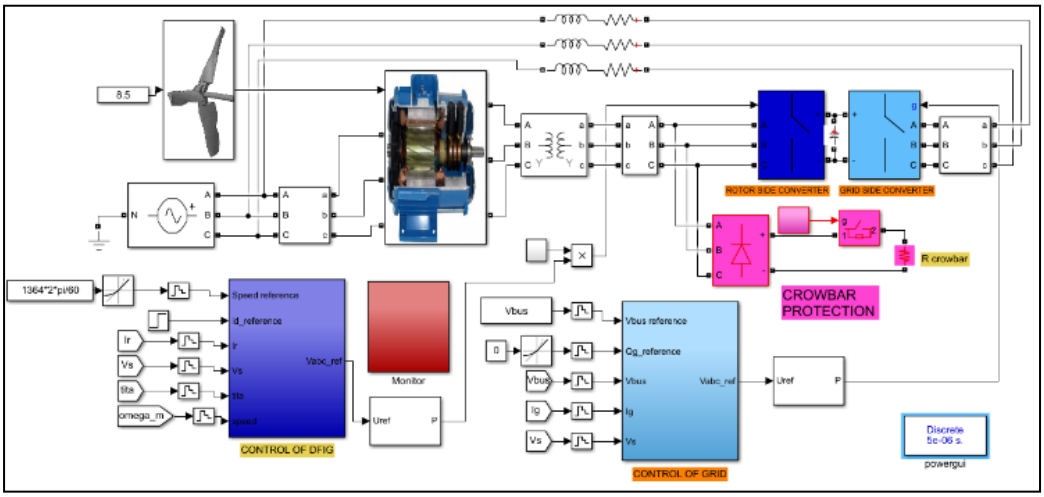


**Fig 7. general simulation of System equipped with crowbar protection**

## Simulation Results

The results obtained by the wind system using vector control, crowbar protection, and power maximization strategies are analyzed. The effectiveness of the crowbar in protecting the GADA is evaluated by examining the performance of the wind turbine under normal and abnormal conditions.

After the symmetrical voltage dips occur at 3 seconds, where the voltage drops to 90% of the nominal voltage, disturbances can be caused when the rotor current (Ir) exceeds the current limit (Irlimit) or when the DC bus voltage (Vbus) exceeds the voltage limit (Vbuslimit). During this time, the crowbar protection is automatically activated by monitoring these two variables (Ir, Vbus). Typically, the current is the first one to exceed its limit. Once the voltage dip is detected, the crowbar protection is activated within 100 milliseconds. The following figure illustrates the events that occur during this process.

The appropriate figures 8-10 illustrates the variations of different variables in the system, accompanied by an attempt to explain the observed changes:

### 1.Variation of current CROWBAR:

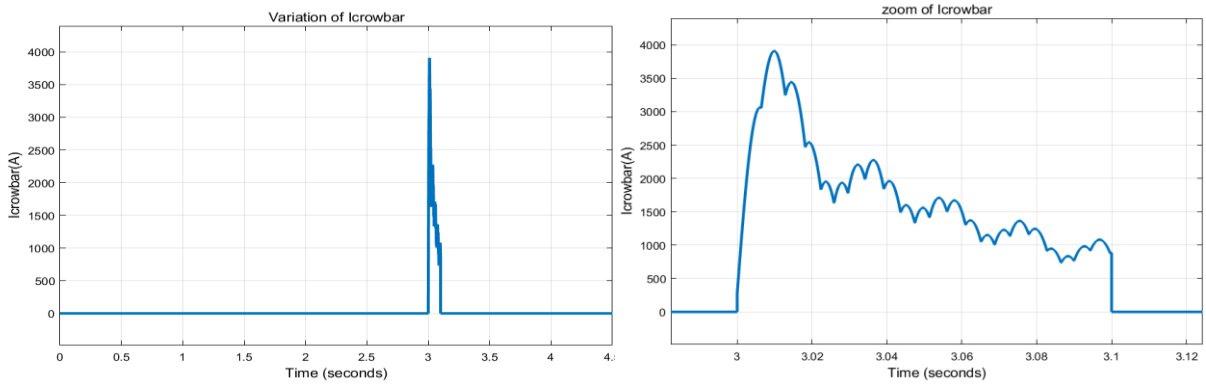

(a1) (a2)

a1) current CROWBAR. a2) Zoom

**Fig 8 . Presentation of current CROWBAR**

## 2.Variation of rotor side converter variables RSC:

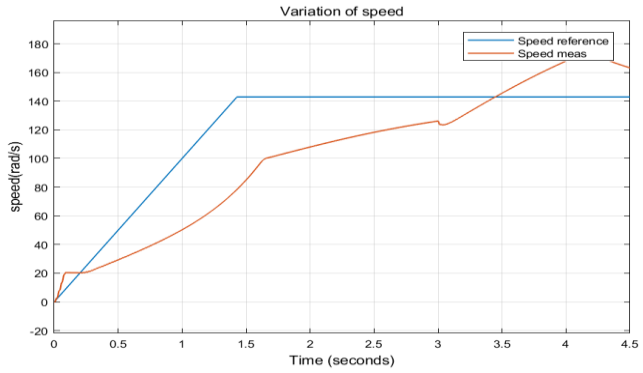


(a)

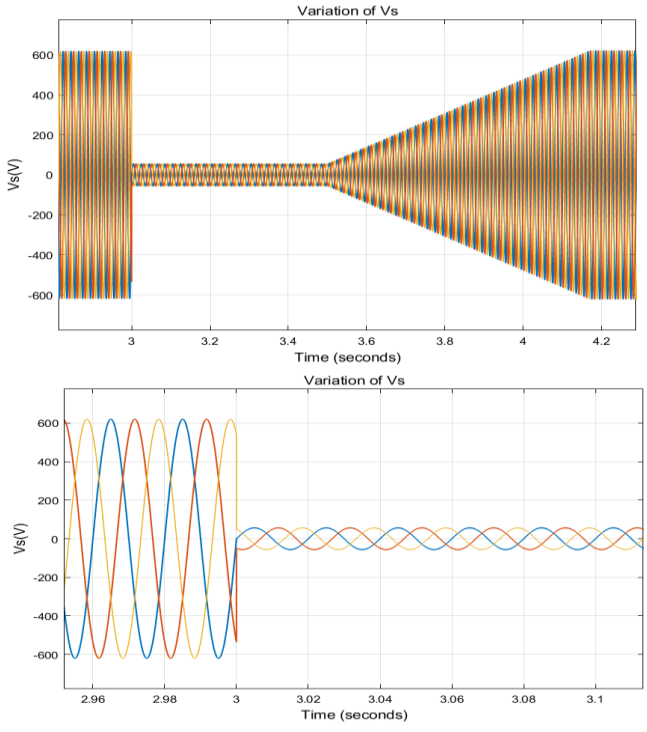


(b1) (b2)

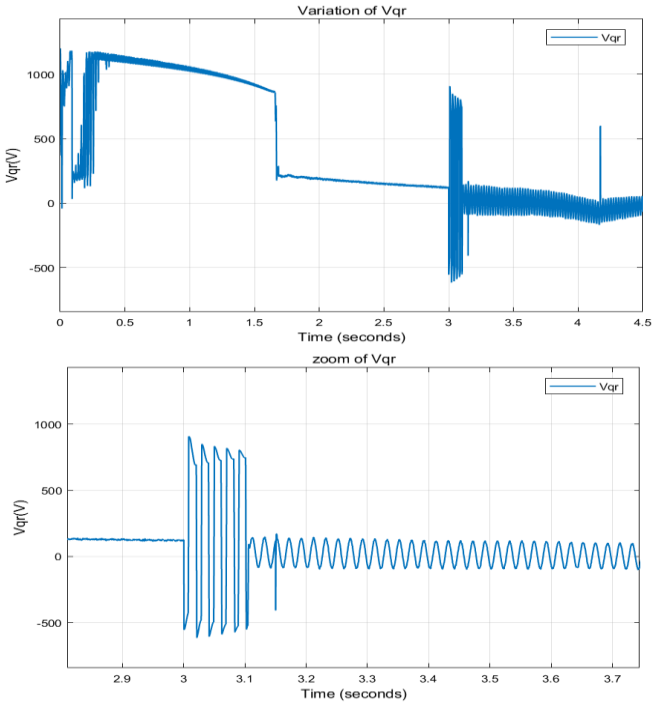
Variation of Vqr
Vqr
Vqr(V)
Time (seconds)
zoom of Vqr
Vqr
Vqr(V)
Time (seconds)

(c1) (c2)

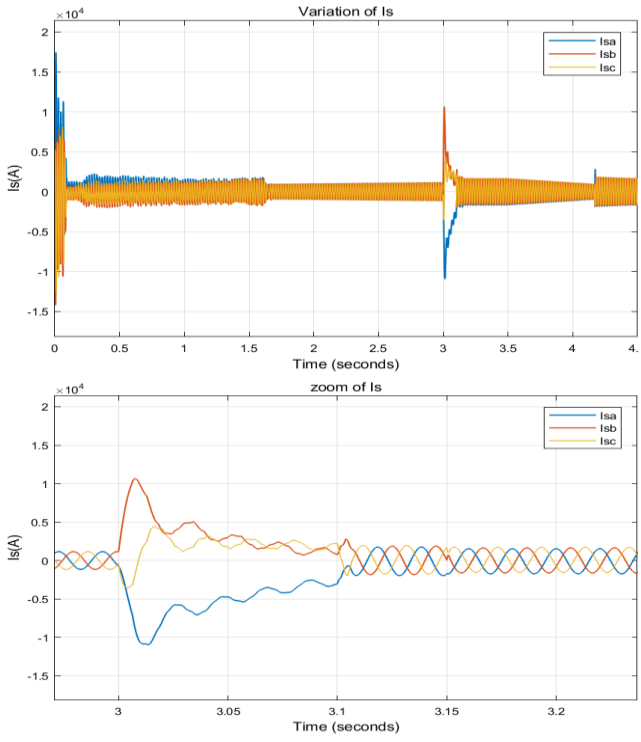
Variation of Is
Isa
Isb
Isc
Is(A)
Time (seconds)
zoom of Is
Isa
Isb
Isc
Is(A)
Time (seconds)

(d1) (d2)

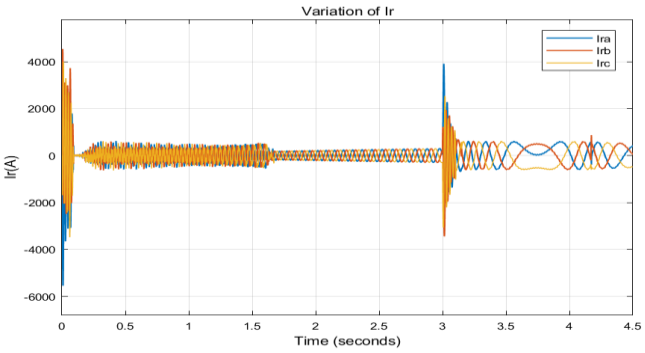
Variation of Ir
Ira
Irb
Irc
Ir(A)
Time (seconds)

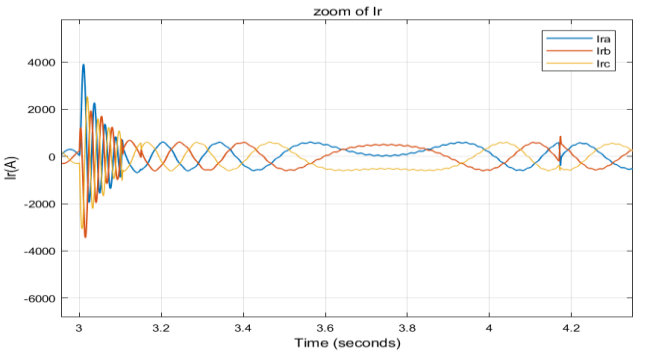
zoom of Ir
Ira
Irb
Irc
Ir(A)
Time (seconds)

(e1) (e2)

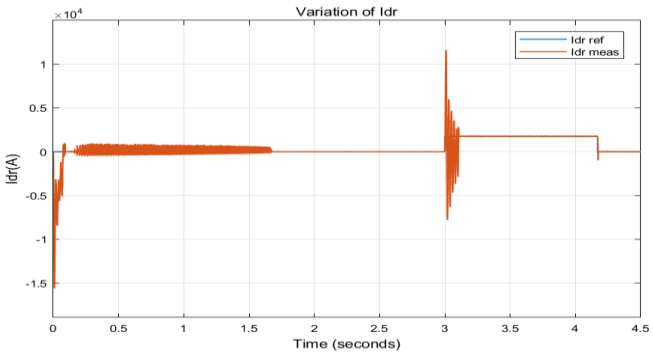
Variation of Idr
Idr ref
Idr meas
Idr(A)
Time (seconds)

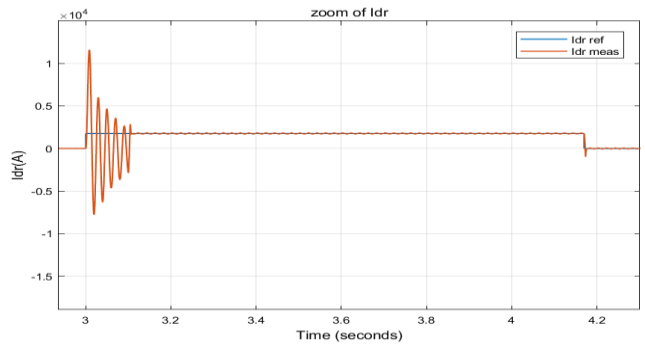
zoom of Idr
Idr ref
Idr meas
Idr(A)
Time (seconds)

(f1) (f2)

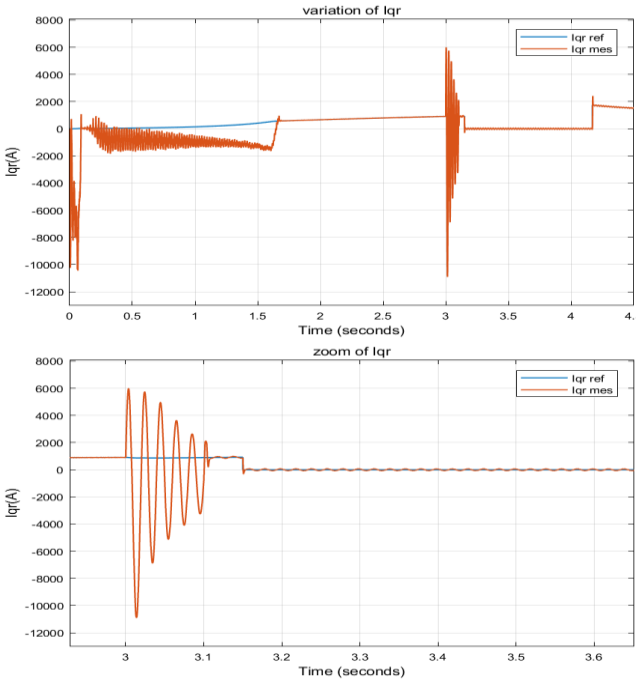
variation of Iqr
Iqr ref
Iqr mes
Iqr(A)
Time (seconds)
zoom of Iqr
Iqr ref
Iqr mes
Iqr(A)
Time (seconds)

(g1) (g2)

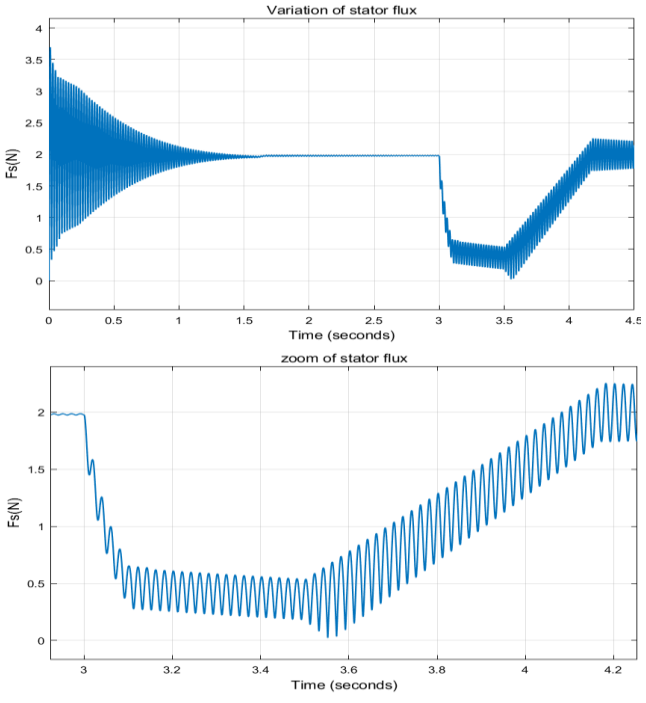
Variation of stator flux
Fs(N)
Time (seconds)
zoom of stator flux
Fs(N)
Time (seconds)

(h1) (h2)

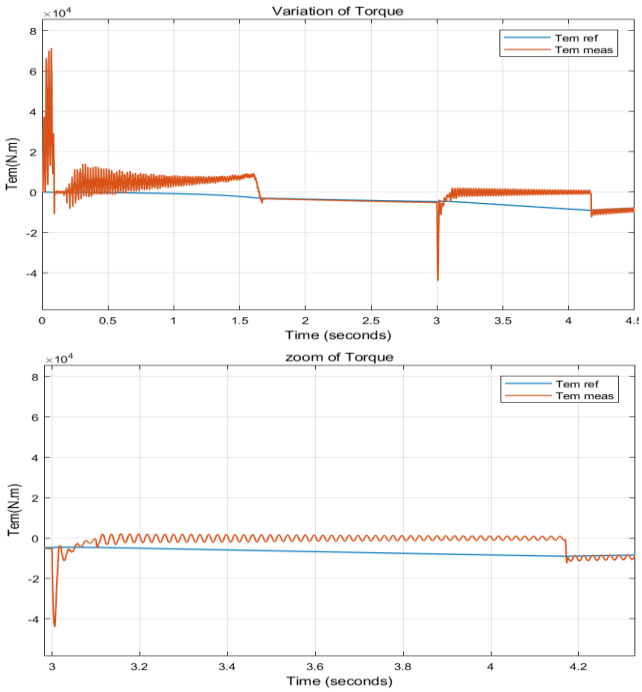


(i1) (i2)

a) Rotor speed,

b1) Vs, Stator voltage, b2) Zoom

c1) Vqr, quadratic rotor voltage, c2) Zoom

d1) Is, Stator current, d2) Zoom

e1) Ir, Rotor current, e2) Zoom

f1) Idr, Direct rotor current, f2) Zoom

g1) Iqr, quadratic rotor current, g2) Zoom

h1) Fs, Stator flux, h2) Zoom

i1) Tem, Torque , i2) Zoom

**Fig 9** . Presentation of different rotor side converter variables **RSC**

**3.Variation of grid side converter variables GSC:**

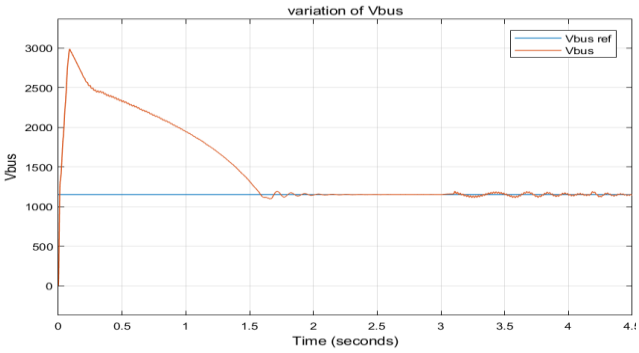
variation of Vbus
Vbus ref
Vbus
Vbus
Time (seconds)

(a1)

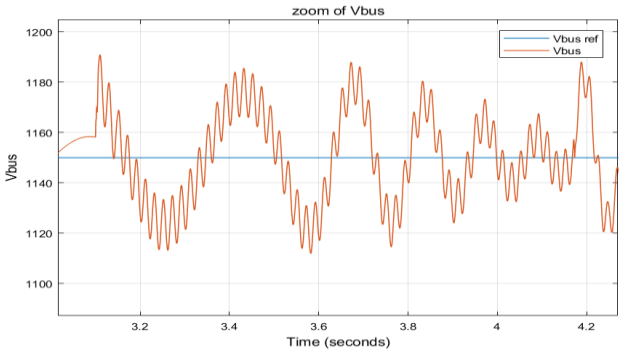
zoom of Vbus
Vbus ref
Vbus
Vbus
Time (seconds)

(a2)

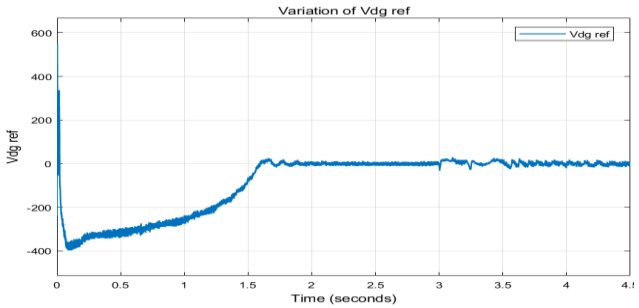
Variation of Vdg ref
Vdg ref
Vdg ref
Time (seconds)

(b)

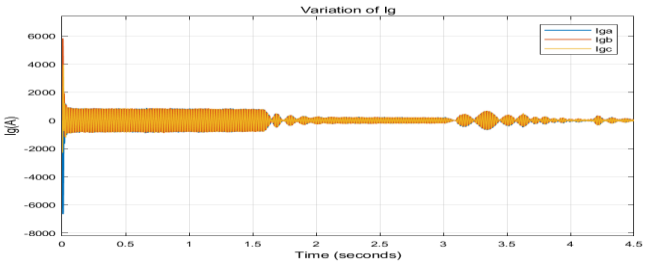
Variation of Ig
Iga
Igb
Igc
Ig(A)
Time (seconds)

(c1)

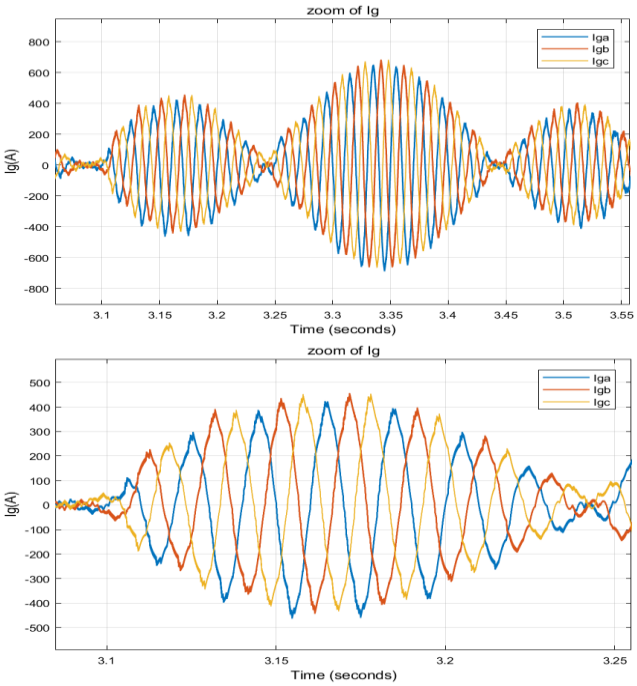
zoom of Ig
Iga
Igb
Igc
Ig(A)
Time (seconds)
zoom of Ig
Iga
Igb
Igc
Ig(A)
Time (seconds)

(c2) (c3)

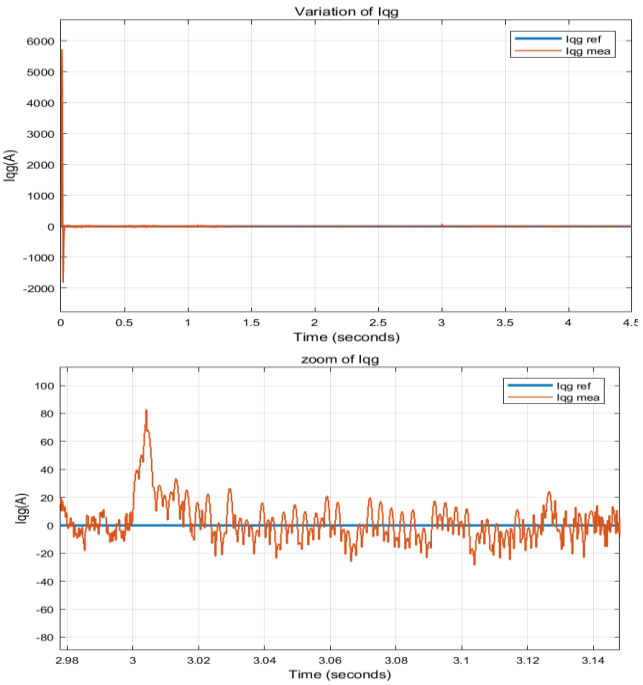
Variation of Iqg
Iqg ref
Iqg mea
Iqg(A)
Time (seconds)
zoom of Iqg
Iqg ref
Iqg mea
Iqg(A)
Time (seconds)

(d1) (d2)

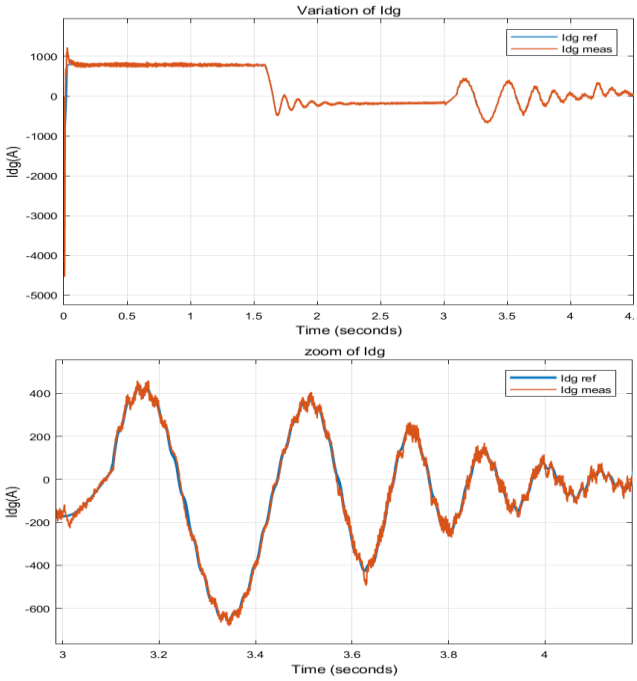


(e1) (e2)

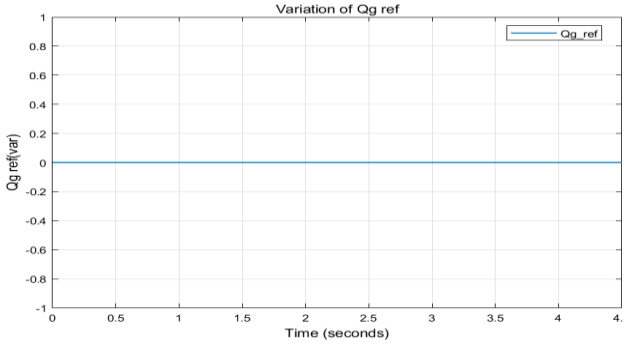


(f)

a1) Vbus, Bus voltage. a2) Zoom

b) Vdg, reference direct grid voltage

c1) Ig, Grid current, c2) Zoom1, c3) Zoom2

d1) Iqg, Quadratic grid current, d2) Zoom

e1) Idg, Direct grid current, e2) Zoom

f) Qg, Grid reactive power.

**Fig 10 . Presentation of different grid side converter variables GSC**

We strive to accurately explain the observed variations of these variables.

Figures 8.a (crowbar) show During this time, the peak current passes through the crowbar resistance and crowbar current variation is faster between (3 and 3.1)s,

In the figures 9.b and 9.d (vs,is) "At 3 seconds, the stator voltages Vs decrease by 90% of the nominal value, and the remaining voltage at the grid is only 10%. Additionally, the stator currents are influenced, reaching a peak at 3 seconds before returning to their sinusoidal form."

The figures 9.h (flux) shows that the flow Oscillates and its value decreases rapidly during the operation of the crowbar, and subsequently returns to its normal value over time."

The figures 9.e (Ir) During voltage dips, the grid voltage temporarily decreases. This can result in a decrease in magnetic flux within the machine, requiring a sudden increase in rotor current to maintain power balance. and compensate for the voltage drop.

At the onset of the voltage dip, At the time of 3s Fugure 9.a (speed), we observe a decrease in rotor speed, and then it rises . This is because the grid voltage decreases, leading to a reduction in the stator voltage of the DFIG. Since the mechanical power provided by the wind remains constant, the rotor speed slows down to maintain power ,We lost speed control, and as a result, the speed decreased until it crossed the synchronous speed (Nr > Ns). At this point, the rotor currents are nearly constant, indicating that we are operating in an hyper synchronous state."

In figures 9.i (torque) It is observed that the peak of electromagnetic torque is associated with the peak of crowbar current, which cannot be avoided. Afterwards, it oscillates around zero before returning to its normal setpoint.". This variation in torque can be attributed to the decrease in grid voltage, which leads to a reduction in magnetic flux and consequently a decrease in the electromagnetic torque developed by the generator. This results in an oscillation of the torque around zero. With a relatively low disturbance rejection time."

Once the voltage dip is resolved and the grid voltage returns to normal, the control strategy of the DFIG adjusts the parameters of the Rotor-Side Converter (RSC) to bring the electromagnetic torque back to its normal setpoint. This ensures stable operation of the system.

Regarding the performance of the rotor side converter, Figures 9.g (iqr) , we can observe that at the beginning of voltage dips, the current Iq is set to zero, which also results in zero torque. However, there are oscillations due to the voltage dips. What happens is that the maximum power point tracking algorithm requires this torque to control the speed."

"During the symmetrical voltage dips required by the grid codes, in Figures 9.f (idr), we have applied a high value of Id rotor current to generate reactive power through the stator by imposing this current component."

In figures 9.c (vqr), the variation of Vqr is similar to the variation of of the current component (Q) Iqr during the disturbance. This can be observed by an increase in amplitude and an oscillation of Vqr around zero

**GSC**

Figures 10.a (VBUS) illustrate the variation of Vbuc, which oscillates around its reference voltage set at 1200 V."

The stability of the voltage across this capacitor is necessary for the proper operation of the system. The control of the capacitor voltage is achieved through the Capacitor Control Regulator (GSC).,

In figures 10.b-10.e , It is observed that the variations of grid currents and voltages (idgrid, iqgrid, vqgrid,) during disturbances follow similar patterns. When a voltage dip occurs, the grid currents and voltages undergo oscillations around their nominal values. Once the voltage dip is over, the control strategies of the system restore the grid currents and voltages to their nominal values, ensuring stable system operation.

Figure 10.f (qg) shows the reactive power, where the imposed reference powers are well followed by the generator. A zero value has been imposed on the reactive power to ensure a unity power factor.

**Conclusion :**

The results obtained in this study demonstrate the impact of symmetrical voltage dips on the performance of the DFIG wind turbine. The analyzed figures reveal variations in electrical and mechanical quantities, as well as the influence of protection and regulation strategies on the system's stability.

During symmetrical voltage dips, the stator voltages decrease significantly, leading to transient variations in stator currents. The rotor currents increase abruptly to compensate for the voltage drop and maintain power balance. These variations can have an impact on the system's stability, particularly on rotor speed and magnetic flux.

Protection strategies, such as the use of crowbar resistances, play a crucial role in maintaining the wind turbine's connection to the grid during symmetrical voltage dips. This ensures continuous energy production and limits transient variations in electrical quantities.

Regulation strategies also contribute to mitigating the effects of disturbances. They help minimize rotor speed variations and maintain stable system operation. Regulation of both rotor-side and grid-side converters is vital for ensuring a fast and effective response to symmetrical voltage dips and maintaining system stability.

The obtained results underscore the importance of optimizing control parameters to ensure optimal performance of the DFIG wind turbine in the presence of electrical disturbances. Recommendations can be formulated to enhance protection and regulation strategies, ensuring system stability and equipment protection.

In conclusion, this study highlights the significance of understanding and managing the effects of symmetrical voltage dips on DFIG wind turbines. The obtained results can be utilized by wind farm designers and electrical grid operators to enhance the reliability and performance of DFIG wind systems, contributing to the effective integration of renewable energies into the electrical grid

**Parameters :**

**Turbine:**

Number of Blades = 3

R=30 m

G=70

**DFIG:**

P= 1.5 MW

p=2

Vdc=1200 V

Rs= 0.012 Ω

Rr= 0.021 Ω

Ls= 0.0137 H

Lr= 0.0136 H

M= 0.0135 H

J=1000 kg.m2

f= 0.0024

## References

[1] Wind Energy Explained: Theory, Design, and Application" by James F. Manwell, Jon G. McGowan, and Anthony L. Rogers: Published in 2010.
[2] Wind Energy Engineering: A Handbook for Onshore and Offshore Wind Turbines" by Trevor M. Letcher: Published in 2017.
[3] Control of Doubly Fed Induction Generators for Wind Turbines" by Edgar N. Sanchez, Riemann Ruiz-Cruz, and Fernando L. Tofoli: Publication date not specified.
[4] Power Converters for Medium Voltage Networks" by Siegfried Heier: Published in 2004.
[5] Wind Turbine Control Systems: Principles, Modelling and Gain Scheduling Design" by Fernando D. Bianchi: Published in 2006.
[6] [Electric Power Systems: A Conceptual Introduction" by Alexandra von Meier: Published in 2006.
[7] Power Systems Analysis and Design" by J. Duncan Glover, Thomas Overbye, and Mulukutla S. Sarma: Published in 2017.
[8] Analysis of Faulted Power Systems" by Paul M. Anderson and Bahman Sanaye-Pasand: Published in 2018.
[9] Wind Energy: Renewable Energy and the Environment" by Vaughn Nelson and Kenneth Starcher: Published in 2013.
[10] J.P. Caron J.P. Hautier. Electrotechnique Modélisation et commande de la machine asynchrone. Presses Universitaires de Strasbourg, 1995.
[11] C. Canudas de Wit. Commande des moteurs asynchrone, Modélisation contrôle vectoriel et DTC. vol.1, Lavoisier, Paris, 2000.
[12] J. Chatelain. Machines Electriques. 1990.
[13] K. Idjdarene A. Tounzi D. Rekioua, T. Rekioua. Vector control of autonomous induction generator taking saturation effect into account. Energy Conversion and Management, 2008.
[14] D. Seyoum C. Grantham, M.F. Rahman. The dynamic characteristics of an isolated self-excited induction generator driven by a wind turbine. IEEE Transactions on Industry Applications, 2003.
[15] A. Hughes. Electric Motors and Drives Fundamentals, Types and Applications. 2005.
[16] Abu-Rub, H., Malinowski, M., & Al-Haddad, K. (2014). Power electronics for renewable energy systems, transportation and industrial applications. John Wiley & Sons Chapter10, pp 179,282.
[17] Abad, G., Lopez, J., Rodriguez, M., Marroyo, L., & Iwanski, G. (2011). Doubly fed induction machine: modeling and control for wind energy generation. John Wiley & Sons.